Med Biol Eng Comput (2011) 49:1437–1445
DOI 10.1007/s11517-011-0801-8

ORIGINAL ARTICLE

Biomechanical comparison of fusionless growth modulation corrective techniques in pediatric scoliosis

Mark Driscoll · Carl-Eric Aubin · Alain Moreau · Stefan Parent

Received: 26 August 2010 / Accepted: 2 July 2011 / Published online: 14 July 2011

Abstract Fusionless growth-sparing implants for the treatment of adolescent idiopathic scoliosis (AIS) attempt to manipulate vertebral growth to restore spinal alignment. This study critically explores different implants utilizing a human spine scoliotic finite element model (FEM). Stainless steel (SS) and shape memory alloy (SMA) staples and flexible tethers were modeled and alternatively integrated around the apex of the convexity of the scoliotic model. Stress profiles over vertebral growth plates were obtained. Two years of growth was simulated with non-instrumented and instrumented models, as curvature changes were quantified. Apical asymmetrical stresses in non-instrumented and instrumented scoliotic models with SS staple, flexible tether, and SMA staple were 0.48, 0.48, 0.23, and 0.33 MPa, respectively. Patient data and non-instrumented model progressed from 28° to 62° of thoracic Cobb angle over 2 years. Simulated projected long-term thoracic Cobb angles of instrumented models are 31° with SS staple, 31° with flexible tether, and 34° with SMA staple. Initial implant compression achieved during instrumentation provided a significant influence on initial and long-term spinal profiles. The developed FEM provides an effective platform with which to explore, critique, and enhance fusionless growth-sparing techniques.

Keywords Scoliosis · Growth modulation · Finite element model · Fusionless devices

M. Driscoll · C.-E. Aubin
École Polytechnique de Montréal, Mechanical Engineering Department, Montreal, Canada

M. Driscoll · C.-E. Aubin · A. Moreau · S. Parent
Research Center, Sainte-Justine University Hospital Center, Montreal, Canada

C.-E. Aubin · S. Parent
Department of Surgery, Faculty of Medicine, Université de Montréal, Montreal, Canada

C.-E. Aubin (✉)
Mechanical Engineering Department, École Polytechnique de Montréal, P.O. Box 6079, Station "Centre-ville", Montreal, QC H3C 3A7, Canada
e-mail: carl-eric.aubin@polymtl.ca

A. Moreau
Department of Stomatology, Faculty of Dentistry, Université de Montréal, Montreal, Canada

A. Moreau
Department of Biochemistry, Faculty of Medicine, Université de Montréal, Montreal, Canada

1 Introduction

Adolescent idiopathic scoliosis (AIS) is characterized by a three-dimensional (3D) deformity of the spine. Consequently, this results in irregular spinal loading and internal stress distribution. These asymmetrical stresses have been quantified in scoliotic spines [17], as well as having been demonstrated utilizing a rigid-body model model and finite-element model (FEM) under various loading techniques [8, 11, 29, 31]. It is generally believed that these irregular forces play a role in the pathomechanism of scoliosis under the Hueter-Volkmann principle, which identifies bone growth-rate dependence on local stress magnitudes [16]. Further, when a scoliotic deformity is coupled with the peak-growth velocity period of adolescents, the severity of the deformation is at a high risk of progression [15].

These conclusions emphasize growth plate stress distribution and remaining spinal growth as important risk

factors to identify, and perhaps exploit, as a means to restore regular alignment to scoliotic spines. Bracing has attempted to address this issue, however, thus far, curve observation and bracing share similar and troubling inconsistencies in preventing the need for surgical intervention involving fusion [7]. In addition, conflicting variability in curvature development continues to limit progressive forecasting, and thus obscures a clinician's ability to adequately select optimal or case-specific treatments.

Alternatively, new methods of intervention, which may be conceived as a form of internal bracing of the spinal column, are being developed for the early treatment of AIS. Fusionless hemi-epiphysiodesis utilizing growth-sparing instrumentation provides an attractive treatment of scoliotic spines. In particular, scoliotic patients undergoing pubertal growth with Cobb angles between 20° and 30° may benefit from this novel approach, as they require surgical intervention at a rate of 70.9 or 100%, if the annual progression exceeds 6° or 10°, respectively [5]. Growth-sparing instrumentation attempts to harness remaining spinal growth in order to manipulate vertebral body geometry in an effort to reverse vertebral wedging in the coronal plane. Such an approach would, in theory, maintain a degree of segmental mobility, allow for a minimally invasive surgery, and effectively impede, halt, or reverse the scoliotic progression.

There are a growing number of registered patents that document the endeavor to turn these theoretical advantages into tangible solutions for the improved treatment of idiopathic scoliosis. These patents consist of conceptual prototypes, as well as implants that have undergone rigorous animal and/or human experimental trials. Examples of the most serious and hopeful among them consist of a rigid stainless steel (SS) staple [37], a flexible tether [3], and a shape memory alloy (SMA) staple [2]. Although these implants vary in rigidity, all are mechanically similar in their attempt to restrict unilateral growth on the convexity of the curvature, which is accomplished by locally increasing stress over vertebral growth plates. Preliminary results obtained with such implants appear promising. Notwithstanding such hopefulness, experimental limitations, and trial differences add significant difficulty in drawing comparative conclusions concerning the various implants' performance, and therefore restrain translation of expectations and optimism for the treatment of AIS.

Thus, the purpose of this biomechanical study is to critically explore methods of fusionless growth modulation in a human scoliotic FEM by quantifying a selected method's ability to manipulate stress distribution over the growth plates, provide immediate corrective influence on spinal alignment, and provide long-term correction via growth modulation.

2 Methods

A normal and a scoliotic FEM of 13-year-old female anterior spines were developed utilizing ANSYS 11.0 (Canonsburg, PA). Both models possess normal sagittal profiles (kyphosis: 34°; lordosis: 44°), however, while the normal model possesses no coronal curvatures, the scoliotic model exhibits a right thoracic curve (Cobb angle of 28°). Anatomical landmarks arose from 3D reconstructive techniques using biplanar radiographs of the two cases providing an accuracy previously validated for mechanical analysis (1.2 ± 0.8 mm for vertebral bodies) [6]. Internal divisions of the models respect physiological proportions from published studies, specifically 0.64 mm cortical shell [9]; 0.62 mm growth plate (immature endplate) [24]; and a nucleus cross-sectional area proportion of 45% [28]. Anterior and posterior longitudinal ligaments cross-sectional areas are 38 and 20 mm^2, respectively [22]. Physiologic divisions include cortical and cancellous bone, growth plate, annulus fibrosis, nucleus pulposus, and anterior and posterior longitudinal ligaments. Linear mechanical properties attributed to each zone respect mean values of respective data from published studies [33] (Table 1). Growth plates consisted of three individual zones conforming to in vivo observation and previously simulated growth models [14, 33] (Fig. 1). Sensitive zone includes reserve, immature proliferative and upper hypertrophic divisions, all of which are responsive to stress sensitivity [23]. Newly formed bone layer consists of lower

Table 1 Mechanical properties of the finite element model

	Young's modulus (MPa)	Poisson's ratio
Vertebral body		
Cortical bone	14,500	0.3
Cancellous bone	400	0.3
Growth plate		
Sensitive zone	12	0.4
Newly formed bone	100	0.3
Transition zone	300	0.3
Intervertebral disc		
Nucleus	2	0.49
Annulus	8	0.45
Ligaments		
Anterior longitudinal	20	0.3
Posterior longitudinal	70	0.3
Implants		
Stainless steel staple	190,000	0.4
Flexible tether	275	0.3
Shape memory alloy staple	80,000	0.3

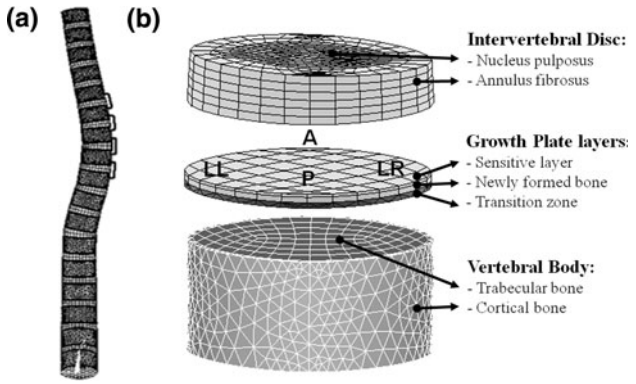

Fig. 1 **a** Postero-anterior view of the instrumented scoliotic finite element model. **b** Vertebral body, intervertebral disc, and detailed growth plate with zones of interest (*A* anterior, *P* posterior, *LL* lateral left, and *LR* lateral right)

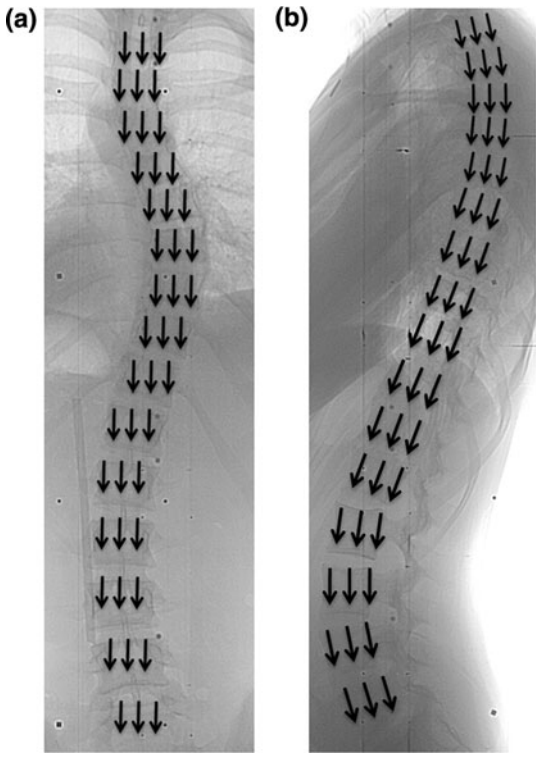

Fig. 2 Representation of load vectors introduced in model with reference to **a** coronal and **b** sagittal planes

hypertrophic region in which bone apposition and calcification occurs. Transition zone represents a gradual increase in rigidities between cartilaginous growth plates and cancellous bone.

The scoliotic model was alternately instrumented with implants over five vertebral bodies centered about the apex (T5–T9). Implant fixation within vertebral bodies was consistently maintained between trials providing each with identical insertion sites modeled as rigid beams. SS staples were provided material properties of surgical SS. Flexible tethers were modeled capable of transmitting tensional force only and assigned material properties associated with 3.5-mm diameter polyethylene. Initial strain of the element (20%) was selected to mimic forces required to realign each vertebral segment under consideration, as practiced under a clinical setting. SMA staples were assigned mechanical properties respective of surgical body temperature Nitinol in its austenite phase. This staple was modeled using weight bearing tensional elements in order to emulate the initial compression force provided by the temperature triggered phase change. Initial strain utilized (5%) followed experimental results for 8 mm staples [34].

Analyses were performed utilizing two parts. The first part consisted of acquiring average longitudinal stress profiles on various areas of interest in the stress sensitive zone of growth plates (Fig. 1). The inferior surface of L5 is constrained in all degrees of freedom, while the superior surface of T1 is constrained to oppose transverse deflections. To simulate body loading, each vertebral body superior surface is submitted to distributed load magnitudes respecting load allocation ratios derived from Schultz [27] and previously employed in scoliotic FEMs of the spine [8, 35] (i.e. 14% body weight over T1 with an additional 2.6% per inferior vertebrae resulting in a cumulative 55.6% over L5). Spinal load vectors in the coronal plane respected gravitational direction (z axis of global coordinate system). Loading in the sagittal plane was maintained tangential to the curve of the spine to insure spinal stability as displayed by the resultant load vectors at each level in Fig. 2. Stress acquisition over these zones was initially performed on the normal FEM and the non-instrumented scoliotic FEMs to collect stress profiles from which to compare the stress manipulative ability of the explored implants. Scoliotic FEM was then alternatively introduced with implants prior to initiation of loading in order to simulate the pre-operative curve reduction obtained in a clinical setting during the lateral decubitus patient positioning [13]. As a result, the scoliotic FEM was instrumented while under a thoracic Cobb angle of 16° (43% reduction over loaded non-instrumented scoliotic model). Once instrumented, the scoliotic FEM was submitted to the adopted spinal loading, while new stress profiles and spinal configuration were recorded. Initial correction provided by the implant was defined by the difference in thoracic Cobb angles between the loaded non-instrumented and instrumented models.

The second part of the analysis involved simulating growth over a 2-year period. The integrated iterative control system begins with application of spinal loading followed by applying calculated growth response to the newly formed bone layer of the growth plates, after which

the geometry of the model is updated. This process is repeated during the simulated growth phase similar to previously explored scoliotic models [8, 35, 36], which is briefly detailed below.

The governing equation, which regulates the level of longitudinal bone growth (G), is based on in vivo correlations acquired from quantifying growth rates under external forces for various animal species [29, 30].

$$G = G_{\mathrm{m}}(1 - \beta(\sigma - \sigma_{\mathrm{m}}))$$

This equation provides the ratio of expected vertebral longitudinal growth rates (G_{m}: 0.8–1.1 mm/year) [25] according to the difference in magnitudes between scoliotic stress (σ) and regular physiological stress (σ_{m}). Sensitivity of the growth algorithm (β) was adjusted to 1.3 MPa^{-1} in order to simulate the scoliotic progression of the selected patient, who progressed more than 10° per year for two consecutive years. Such corroborative calibration ensured patient-specific progression which, in turn, served as a constant platform to compare devices. Finally, 2 years of spinal growth was simulated for the non-instrumented and instrumented models while changes in coronal Cobb angles were recorded.

The final step of the study consisted of performing several sensitivity analyses in order to interpret the influence of the numerical assumption adopted in the spine and implant models. This included repeating all simulations under different loading directions (tangential to curve and gravitational in both sagittal and coronal planes), initial strains or pre-tension values assigned to flexible tethers and SMA staples (modified by ±25% of their respective values), and implant insertion sites (varied superiorly and inferiorly with respect to the intervertebral disc as shown in Fig. 3). Initially, the influence of these variables on growth plate stress distribution was explored. The variables that posed significant stress differences were further pursued and their manipulation of the thoracic Cobb angle following 2 years of simulated growth was investigated.

3 Results

Stress distribution over vertebral growth plate returned unique profiles for each simulation. The apex (T7) provided the most insightful depiction of the variability invoked by the presence of the explored implants (Fig. 4). Standard stress profile, obtained from the normal spine model, returned symmetric lateral profiles. Lateral stresses registered in the left (LL) and right (LR) areas were 0.35 MPa collectively, while the average anterior (A, ALL, and ALR) and posterior (P, PLL, and PLR) stresses obtained were 0.41 and 0.16 MPa, respectively. Stress profile of the non-instrumented scoliotic right thoracic model returned similar stress profiles to the normal model with respect to anterior (A) and posterior (P) zones,

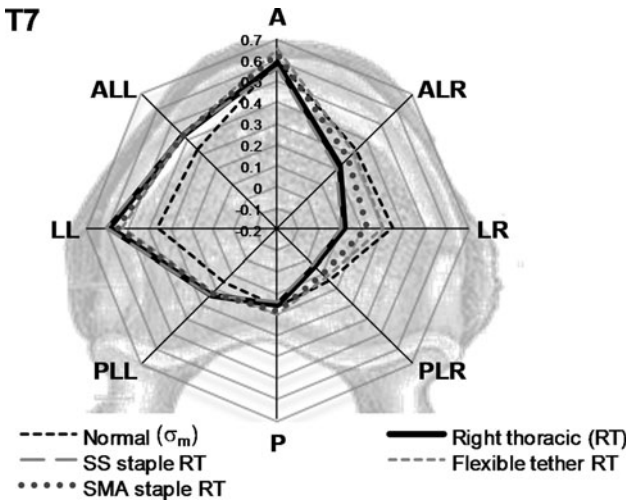

Fig. 4 Longitudinal (normal) stress in MPa profiles over apical vertebral growth plate (T7) of normal model, right thoracic scoliotic model and right thoracic scoliotic model with implants over anterior (A), anterior lateral right (ALR), lateral right (LR), posterior lateral right (PLR), posterior (P), posterior lateral left (PLL), lateral left (LL), and anterior lateral left (ALL)

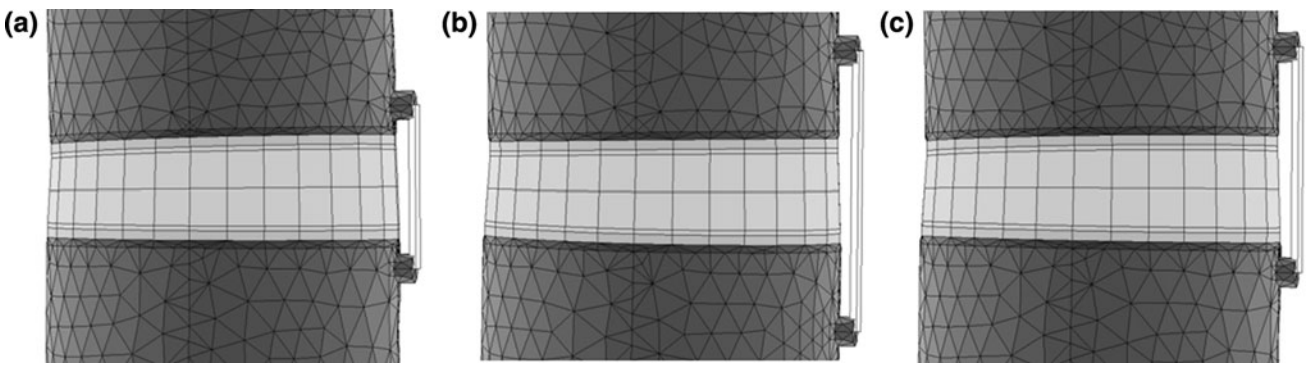

Fig. 3 Explored implant insertion sites **a** adjacent to growth plates, **b** short distance apart from growth plates, and **c** superior offset with respect to intervertebral disc

whereas concave (LL) and convex (LR) profiles demonstrated asymmetrical loading within the scoliotic spine. More specifically, the concave portion of the apical growth plates yielded a stress of 0.60 MPa, whereas stress in the convex section measured 0.12 MPa. This translates into an asymmetrical loading of 0.48 MPa. The instrumented right thoracic models consistently shared similar anterior and posterior profiles with both the normal and right thoracic models. In addition, lateral stress profiles (LL and LR) in instrumented models clearly displayed the implants' attempt to return stress distribution to regular conditions, as measured in the normal model. The scoliotic model instrumented with the SS staple had little influence on stress profiles, as they were similar to those observed in the non-instrumented scoliotic model. Introduction of the flexible tether into the right thoracic model reduced slightly concave stress to 0.53 MPa, and increased significantly convex stress to 0.30 MPa in comparison to the non-instrumented scoliotic model. In turn, these alterations adjusted the magnitude of asymmetrical loading to 0.23 MPa. The scoliotic FEM instrumented with the SMA staple provided similar but less effective results to the flexible tether. Apical concave and convex stresses were measured at 0.55 and 0.22 MPa, respectively, thereby reducing the asymmetrical loading to 0.33 MPa.

The simulated growth of the non-instrumented scoliotic model corroborated closely with progressive sequence of the patient data, as demonstrated in Fig. 5 and quantitatively summarized in Fig. 6. The FEM proposed a Cobb angle progression from 28° to 42° in the first year, followed by an increase to 62° after 2 years—whereas the selected patient had an initial thoracic Cobb angle of 30°, which became 41° and 62° after 1 and 2 years, respectively, as a result of inadequate brace treatment. After this point, the patient underwent posterior fusion resulting in a final thoracic curve of 24°.

The simulated scoliotic model instrumented with the SS staple displayed a negligible initial correction over the non-instrumented model; however, growth results show the implant would establish a Cobb angle of 29° after 1 year, followed by 31° after 2 years. As a result, the SS staple confined progression to 3° (or a relative increase of 11%) over 2 years of growth. The scoliotic model instrumented with the flexible tether provided an initial correction that resulted in a post-operative curvature of 23°. This value translates into a 5° (or 18%) initial reduction when compared to the original configuration of the non-instrumented model. After 1 and 2 years of simulated growth dynamics, the tethered model progressed to a curvature of 27° and 31°, respectively. Finally, the SMA staple provided a mild initial correction of 3° (or 10%) over the non-instrumented scoliotic model. The long-term post-operative influence of this technique predicted a thoracic curve of 29° after 1 year and 34° after 2 years. To summarize (Fig. 6), after 2 years, the curve of the patient under consideration and the non-instrumented scoliotic model progressed by 34° (120%) with respect to the initial scoliotic curvature, whereas the instrumented scoliotic model progressed by 3° (11%), 3° (11%), and 6° (21%) when correspondingly introduced with the SS staple, flexible tether, and SMA staple.

Results from the sensitivity analyses with regards to the implant insertion site proved to be robust and had <5% influence on the magnitude of asymmetrical growth plate stress. On the contrary, the direction of loading proved to have important implications on growth plate stress profiles. Namely, the gravitation loading in both planes invoked a 28% greater asymmetrical stress than reported above. However, in order to couple the progression of the FEM

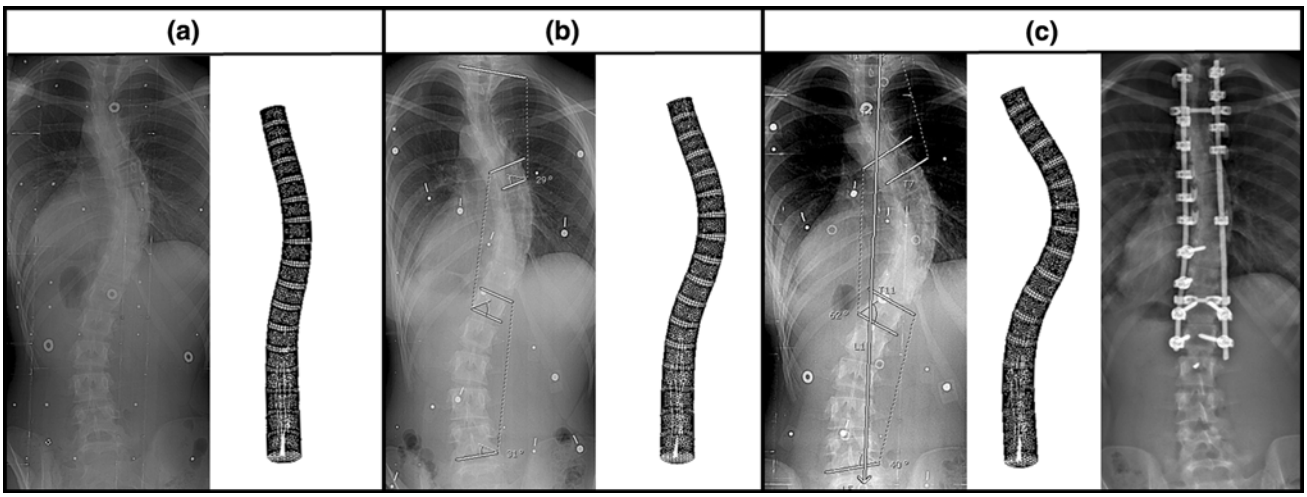

Fig. 5 Patient radiographs and non-instrumented scoliotic model at **a** 13 years, **b** 14 years, and **c** 15 years and post-operative radiograph following posterior fusion

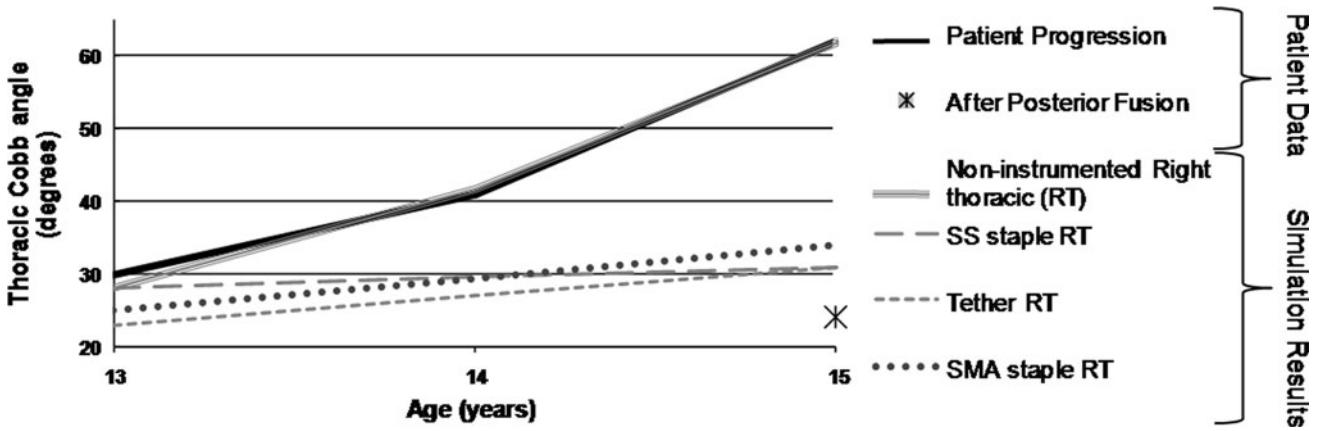

Fig. 6 Progressive results of patient, non-instrumented FEM and instrumented FEMs

with the patient data, the sensitivity parameter (β) was reduced to 0.6. Due to this corroborative modification to the underlying algorithm, the long-term influence of the explored implants on spinal alignment showed insignificant transformations to spinal configuration when compared to those expressed above. Finally, initial tension attributed to the flexible tether and SMA staple revealed conclusive impact in view of their correction of the scoliotic model. More specifically, using $\beta = 1.3$ with a tangential loading while varying the initial strains $\pm 25\%$ led to a 2 year thoracic Cobb angle $30.6 \pm 8.7°$ (SD) with the flexible tether and $33.3 \pm 5.2°$ with the SMA staple. Under similar conditions, using a $\beta = 0.6$ and gravity loading, returned $31.6 \pm 4.0°$ with the flexible tether and $33.6 \pm 3.7°$ with the SMA staple.

4 Discussion

Fusionless growth-sparing approaches for the treatment of AIS were compared utilizing a scoliotic FEM of the spine with integrated growth dynamics. Results suggest these methods as a suitable solution to effectively reduce asymmetrical loading of vertebral growth plates and provide immediate post-operative correction. Moreover, the explored methods achieved long-term growth modulation resulting in reduced scoliotic progression.

Fusionless growth-sparing implants should seek to eliminate, if not reverse, asymmetrical loading of vertebral growth plates. Introduction of implants into the scoliotic model confirmed the ability of the convex lateral approach to reduce asymmetrical loading of vertebral growth plates, an attribute of scoliotic spines believed to play an important role in its progressive pathomechanism [32]. However, this biomechanical analysis also demonstrated the difficulty of the tested implants to establish sufficient control over segmental stresses, which coincides with their struggle to achieve convincing long-term curvature correction. In turn, these results may account for the inability of these methods to stimulate contralateral growth as previously observed during in vivo studies of the flexible tether and the SMA staple [4]. Reversal of vertebral wedging, by means of altered loading, has previously been achieved, suggesting vertebral growth is not permanently affected by abnormal stress conditions [18]. Therefore, adequate control of growth plate stress distribution via fusionless growth-sparing methods may effectively reverse vertebral wedging, leading to long-term and permanent curvature correction.

Stress predictions, provided by the developed FEM, corroborated with relevant studies. The growth plate stress profile of the normal (non-scoliotic) model in this analysis predicted an average of 0.30 MPa, a value compatible to in vivo human studies measuring mean standing lumbar disc (adjacent to the endplate) stresses of 0.5 [38] and 0.27 MPa [27]. Scoliotic asymmetrical loading obtained herein also agree with measurements of asymmetrical stress distribution around the apical segment of laterally positioned scoliotic patients with mean concave/convex differences of 0.38 ± 0.32 MPa [17]. Alternatively, Stokes reported concave/convex differences in the order of 0.1 MPa [29] using a rigid-body model of the lumbar spine, which may account for the differences.

The SS staple, flexible tether, and SMA staple displayed the ability to significantly reduce scoliotic progression that would have otherwise occurred (Fig. 6). The SS staple achieved reliable growth modulation through its high rigidity (a characteristic that dictates the passive resistance of the device toward expansion granted by vertebral growth). Similar to in vivo porcine trials using SS staples [37], this study reported no immediate post-operative influence on spinal curvature. Such study showed the SS

staple's ability to induce an average coronal Cobb angle of 16.4° (±5.4) after 8 weeks following instrumentation. However, the inverse method (creation of scoliosis on a healthy model) was used. Therefore, no corroborative conclusions of long-term influence may be drawn, as this manuscript explored the percentage of correction achieved in a scoliotic spine. In addition to offering a passive resistance to growth, the flexible tether provided an initial force aimed at altering local segmental load distributions. The flexible tether and the SMA staple have been previously examined on experimentally induced scoliotic goat spines [3]. On average, after 12–16 weeks, the flexible tether provided an initial correction of 15.5% and a long-term change from 73.4° to 69.9°, or a correction of 4.8%. In the same study, the SMA trial led to an average initial correction of 1.5% followed by a long-term progression from 77.3° to 94.3° or a 22% increase. In a human clinical trial of the SMA staple, 13% of instrumented patients having an average pre-operative curves of 33° (20°–41°) progressed by ≥10° or 30%, whereas mixed results were achieved with respect to the remainder of the group, resulting in moderate or no progression [2].

An important difference between these in vivo studies is that, in reference to the induced scoliotic goat trial [3], a control group was used to monitor non-instrumented progression. This control group led to an average coronal Cobb angle increase from 79.5° to 96.8°, thus, establishing a progressive model on which to analyze implants that seek to reverse this effect. Whereas human pre-pubertal curves between 21° and 30° have a high progressive variability [5], making human clinical trials a difficult platform on which to judge the long-term success of an implant. Therefore, the analysis of such methods on a controlled finite element environment provides a suitable platform to derive relative conclusions that may be used to explain previously obtained in vivo results and to predict the feasibility of or optimize new concepts prior to in vivo testing.

Limitations of this FEM study include assumptions associated with spinal loading, which is still insufficiently understood. Loading and boundary conditions were selected to best predict the resultant force vectors that arise from gravitational and muscular forces. To address these uncertainties, a sensitivity analysis was performed to explore the influence of these assumptions. This analysis supported conclusions expressed in this article, as relative distinctions achieved by the implants proved to be consistent under different loading conditions. Only the vertebral bodies were modeled, since it is known to support a convincing majority of compressive loads [1]. Further, the relative motion between vertebrae was monitored to ensure segmental motion remained within physiologic range. Moreover, it was previously demonstrated that irregular pedicle growth did not produce scoliotic curves in a FEM [12]. Nevertheless, the authors recognize that if a contact between posterior elements occurred it may influence local relative displacements between adjacent segments. Although, the iterative control system governing growth dynamics relies on correlation derived from animal species [30], it has been previously modeled to predict realistic rates of scoliotic progression [29, 35]. This biomechanical comparison study focused on the device's ability to manipulate coronal profile while scoliotic deformities are defined by a 3D deformity. To date, fusionless devices focus on the coronal plane deformity and, perhaps, they should also seek to fully address the complexity of the deformity as observed in intermediate or advanced scoliotic curves. The reported results of this manuscript were obtained by isolating selected variables in order to draw relevant comparisons between fusionless methods. However, the authors recognize that in a clinical setting these methods may be subject to mild alterations with respect to insertion sites. In order to address this concern, implant location was varied to represent possible disparity (Fig. 3) and had a minute influence on the previously reported results. Conversely, initial strains attributed to the flexible tether and SMA staple significantly influenced their impact on curvature progression. Nonetheless, the sensitivity of this parameter is not believed to encumber the reported results as its influence was mechanically instinctive. In contrast, recognition of the significance of this factor may in part described the variability observed during in vivo trials of these devices or perhaps be exploited to further optimize their performance.

Although not explored in this analysis, the influence on the health of intervertebral discs must not be neglected, considering that these concepts are developed for pediatric use. Such apprehension is supported by the observation of irregular stress profiles within the growth plates—a phenomenon believed to promote disc degeneration. Implicated researchers have explored this issue and found various stress-induced or hypomobility-related changes in the discs of instrumented segments [10, 21]. In an attempt to address this concern, a fusionless growth-sparing mini-staple has subsequently been developed that does not alter the mechanical environment of the intervertebral discs [26].

The ability to identify patients at risk of progression prior to the onset of peak-growth velocity (currently being pursued by Moreau et al. [19, 20]) and improved stress/growth control would justify and complement this method of early intervention that attempts to correct or limit expected scoliotic progression. Despite the fact that the pathomechanism of scoliosis is likely multi-factorial, fusionless growth-sparing instrumentation provides many biomechanical advantages over conventional treatments. However, several potential improvements remain to be

considered. The use of a finite element platform presents a valuable medium to explore, compare, and, perhaps, improve on methods seeking to corrected spinal deformities via fusionless growth sparring instrumentation.

Acknowledgments Funded by the Natural Sciences and Engineering Research Council of Canada (Industrial Research Chair Program with Medtronic of Canada) and the Canada Research Chair Program.

References

1. Adams M, Hutton W (1980) The effect of posture on the role of the apophysial joints in resisting intervertebral compressive forces. J Bone Joint Surg Br 62(3):358–362
2. Betz R, Andrea L, Mulcahey M, Chafetz R (2005) Vertebral body stapling procedure for the treatment of scoliosis in the growing child. Clin Orthop Relat Res 434:55–60
3. Braun J, Akyuz E, Ogilvie J, Bachus K (2005) The efficacy and integrity of shape memory alloy staples and bone anchors with ligament tethers in the fusionless treatment of experimental scoliosis. J Bone Joint Surg Am 87(9):2038–2051
4. Braun J, Hunt K, Sorenson S, Ogilvie J (2007) Can fusionless scoliosis surgery reverse the Hueter-Volmann effect? In: 42nd annual meeting scoliosis research society, Edinburg, Scotland
5. Charles Y, Daures J, de Rosa V, Dimeglio A (2006) Progression risk of idiopathic juvenile scoliosis during pubertal growth. Spine 31(17):1933–1942
6. Delorme S, Petit Y, de Guise J, Aubin CE, Dansereau J (2003) Assessment of the 3-D reconstruction and high-resolution geometrical modeling of the human skeletal trunk from 2-D radiographic images. IEEE Trans Biomed Eng 50(8):989–998
7. Dolan L, Weinstein S (2007) Surgical rates after observation and bracing for adolescent idiopathic scoliosis: an evidence-based review. Spine 32(19S):91–100
8. Driscoll M, Aubin CE, Moreau A, Villemure I, Parent S (2009) The role of concave–convex biases in the progression of idiopathic scoliosis. Eur Spine J 18:180–187
9. Edwards T, Zheng Y, Ferrara L, Yuan H (2001) Structural features and thickness of the vertebral cortex in the thoracolumbar spine. Spine 26(2):218–225
10. Hunt H, Braun J, Christensen B (2007) The effect of two clinically relevant fusionless scoliosis implant strategies on the health of the intervertebral disc. In: 42nd Annual meeting scoliosis research society, Edinburgh, Scotland
11. Huynh AM, Aubin CE, Mathieu P, Labelle H (2007) Simulation of progressive spinal deformities in Duchenne muscular dystrophy using a biomechanical model integrating muscle and vertebral growth modulation. Clin Biomech 22:392–399
12. Huynh AM, Aubin CE, Rajwani T, Bagnall K, Villemure I (2007) Pedicle growth asymmetry as a cause of adolescent idiopathic scoliosis: a biomechanical study. Eur Spine J 16:523–529
13. Lalonde N, Villemure I, Pannetier R, Parent S, Aubin CE (2010) Biomechanical modeling of the lateral decubitus posture during corrective scoliosis surgery. Clin Biomech 25(6):510–516
14. Lin H, Aubin CE, Parent S, Villemure I (2009) Mechanobiological bone growth: comparative analysis of two biomechanical modeling approaches. Med Biol Eng Comput 47(4):957–966
15. Little D, Song K, Katz D, Herring J (2000) Relationship of peak height velocity to other maturity indicators in idiopathic scoliosis in girls. J Bone Joint Surg 82(5):685–693
16. Mehlman C, Araghi A, Roy D (1997) Hyphenated history: the Hueter-Volkmann law. Am J Orthop 26:798–800
17. Meir A, Fairbank J, Jones D, McNally D, Urban J (2007) High pressures and asymmetrical stresses in the scoliotic disc in the absence of muscle loading. Scoliosis 2:article 4
18. Mente P, Aronsson D, Stokes I, Iatridis J (1999) Mechanical modulation of growth for the correction of vertebral wedge deformities. J Orthop Res 17:518–524
19. Moreau A, Franco A, Azedine B, Rompre P, Turgeon I, Bagnall K, Poitras B, Labelle H, Rivard C, Grimard G, Ouellet J, Parent S, Larouche G, Lacroix G (2008) Elevated plasma factor P is involved in AIS onset and curve progression. In: SRS 43rd annual meeting scoliosis research society, Salt Lake City
20. Moreau A, Wang D, Forget S, Azeddine B, Angeloni D, Fraschini F, Labelle H, Poitras B, Rivard C, Grimard G (2004) Melatonin signaling dysfunction in adolescent idiopathic scoliosis. Spine 29(16):1772–1781
21. Newton P, Farnsworth C, Faro F, Mahar A, Odell T, Mohamad F, Breisch E, Fricka K, Upasani W, Amiel D (2008) Spinal growth modulation with an anterolateral flexible tether in an immature bovine model. Spine 23(7):724–733
22. Polikeit A, Ferguson S, Nolte L, Orr T (2003) Factors influencing stresses in the lumbar spine after the insertion of intervertebral cages: finite element analysis. Eur Spine J 12:413–420
23. Price J, Oyajobi B, Russell R (1994) The cell biology of bone growth. Eur J Clin Nutr 48(Suppl 1):131–149
24. Roberts S, Menage J, Urban J (1989) Biochemical and structural properties of the cartilage end-plate and its relation to the intervertebral disc. Spine 14(2):166–174
25. Sarwark J, Aubin CE (2007) Growth considerations of the immature spine. J Bone Joint Surg Am 89(Suppl 1):8–13
26. Schmid E, Aubin CE, Moreau A, Sarwark J, Parent S (2008) A novel fusionless vertebral physeal device inducing spinal growth modulation for the correction of spinal deformities. Eur Spine J 17(10):1329–1335
27. Schultz A, Andersson G, Ortengren R, Nachemson A (1982) Loads on the lumbar spine. Validation of a biomechanical analysis by measurement of intradiscal pressures and myoelectric signals. J Bone Joint Surg 64(5):713–720
28. Shirazi-Adl A, Shivastava S, Ahmed A (1984) Stress analysis of the lumbar disc-body unit in compression: a three dimensional nonlinear finite element study. Spine 9(2):120–134
29. Stokes I (2007) Analysis and simulation of progressive adolescent scoliosis by biomechanical growth simulation. Eur Spine J 16:1621–1628
30. Stokes I, Aronsson D, Dimock A, Cortright V, Beck S et al (2006) Endochondral growth in growth plates of three species at two anatomical locations modulated by mechanical compression and tension. J Orthop Res 10:1327–1333
31. Stokes I, Gardner-Morse M (2004) Muscle activation strategies and symmetry of spinal loading in the lombar spine with scoliosis. Spine 29(19):2103–2107
32. Stokes I, Spence H, Aronsson D, Kilmer N (1996) Mechanical modulation of vertebral body growth: implications for scoliosis progression. Spine 21:1161–1167
33. Sylvestre PL, Villemure I, Aubin CE (2007) Finite element modeling of the growth plate in a detailed spine model. Med Biol Eng Comput 45(10):977–988
34. Tremblay M (2004) Caractérisation expérimentale de la modulation de croissance vertébrale à l'aide d'agrafes à mémoire de forme pour la correction de la scoliose idiopathique: étude de faisabilité. Master thesis, École Polytechnique de Montréal
35. Villemure I, Aubin CE, Dansereau J (2002) Simulation of progressive deformities in adolescent idiopathic scoliosis using a biomechanical model integrating vertebral growth. J Biomed Eng 124:784–790
36. Villemure I, Aubin CE, Grimard G, Dansereau J, Labelle H (2001) Progression of vertebral and spinal three-dimensional

deformities in adolescent idiopathic scoliosis: a longitudinal study. Spine 26(20):2244–2250
37. Wall E, Bylski-Austrow D, Kolata R, Crawford A (2005) Endoscopic mechanical spinal hemiepiphysiodesis modifies spine growth. Spine 30(10):1148–1153
38. Wilke H, Neef P, Caimi M, Hoogland T, Claes L (1999) New in vivo measurements of pressures in the intervertebral disc in daily life. Spine 24(8):755–762